DISLOCATION ANALYSIS OF PENETRATION IN SATURATED POROUS MEDIA

By Derek Elsworth,[1] Associate Member, ASCE

ABSTRACT: Solution is presented for the fluid-pressure response surrounding insertion of a continuous, moving point dislocation within an initially saturated porous-elastic medium. Included in the presentation is a unified framework for the analysis of penetration-generated pore pressures in soils for partially drained states and an exposition of the overt penetration rate dependence of pore-pressure generation and dissipation. Scaling parameters for data reduction are returned as a natural consequence. The analysis allows rational determination of permeability and consolidation coefficients in situ. Postarrest pore-pressure dissipation at the tip enables C_V to be determined independently. Nonuniqueness in pore-pressure dissipation along the shaft precludes independent determination of consolidation behavior.

INTRODUCTION

The potential application of field penetrometer testing in the determination of in-situ consolidation behavior of soils has been previously recognized (Janbu and Senneset 1974; Wissa et al. 1975; Torstensson 1975; Jones and Van Zyl 1981; Battaglio 1981). Of critical interest in the rational interpretation of data are the mechanisms by which pore pressures are generated around the penetrometer tip as a function of the prescribed, assumed, or measured undrained strain field. The strain field may be evaluated from consideration of the kinematic failure mechanisms, either disregarding (Baligh and Scott 1976) or including (Drescher and Kang 1987) self-weight, and from expanding cavity theories in cohesive soils (Ladanyi 1963; Baligh 1985; Tumay et al. 1985; Acar and Tumay 1986). Instantaneous pore-pressure distributions may be recovered through use of appropriate pore-pressure parameters (Skempton 1954; Biot and Willis 1957). Gupta and Davidson (1986) proposed a model based on undrained pore-pressure generation around an advancing series of inflated spherical cavities in an elastic, perfectly plastic soil. To prevent violation of the superposition principle, the analysis was undrained until penetration arrest. In soils exhibiting moderate permeability, however, and for reduced penetration rates, the potential for concurrent dissipation behind the process zone of the tip must be accommodated.

Complete comprehension of the major factors influencing pore-pressure generation and dissipation around a progressing penetrometer tip is a necessary prerequisite to aid rational interpretation of piezocone data. Of direct interest are the dynamic factors controlling the time required to reach a steady pore-pressure field and the resulting magnitude of generated pore pressures; the interdependence of both penetration rate and the time to cone arrest in influencing the morphology of the surrounding fluid-pressure bulb, dissipation processes, and rates; methods by which acquired pressure records may

[1]Asst. Prof., Dept. of Mineral Engrg., Pennsylvania State Univ., University Park, PA 16802.

Note. Discussion open until July 1, 1991. To extend the closing date one month, a written request must be filed with the ASCE Manager of Journals. The manuscript for this paper was submitted for review and possible publication on August 24, 1989. This paper is part of the ***Journal of Engineering Mechanics***, Vol. 117, No. 2, February, 1991. ©ASCE, ISSN 0733-9399/91/0002-0391/$1.00 + $.15 per page. Paper No. 25504.

be best used to independently determine in-situ permeabilities and compressibilities, as opposed to consolidation parameters alone; and the identification of appropriate parametric groupings governing the concurrent processes of pore-pressure generation and dissipation that maximize the utility of the acquired data. Motivated by these factors, a solution is developed in the following for a point dislocation of constant strength moving within an isotropic, saturated, porous-elastic medium. The analogy with cone penetration is direct.

Moving Point Dislocation

A direct analogy exists between penetration by an amorphously tipped rod and the behavior of a normal dislocation that moves in space and leaves a remnant linear void along the traveled pathway. Conceptually, it is most convenient to choose a fixed-coordinate system located at the head of a penetrometer, past which the elastic medium moves at uniform rate U (in the positive x-direction), as illustrated in Fig. 1. Consider a dislocation at the origin of this coordinate system of volumetric magnitude V. Dislocation rate v may be defined as $V = vd\tau$, in which $d\tau$ is a differentially small time increment. For all times $t \geq 0^+$, a point dislocation is introduced at the origin at the rate v per unit time and the surrounding medium moves parallel to the x-direction at velocity U. The position of a point located at coordinates x, y, and z at current time t would have been $[x - U(t - \tau), y, z]$ at time τ. Under these conditions, solution for a point-normal dislocation (Cleary 1977) may be described

$$p - p^s = \frac{C_V v d\tau}{4\pi \bar{R}^3} \frac{\mu}{k} \left(\frac{\bar{\xi}^3}{2\sqrt{\pi}} e^{-\bar{\xi}^2/4} \right) \quad \text{..... (1)}$$

with

$$\bar{\xi} = \frac{\bar{R}}{\sqrt{C_V(\tau - \tau)}} \quad \text{..... (2a)}$$

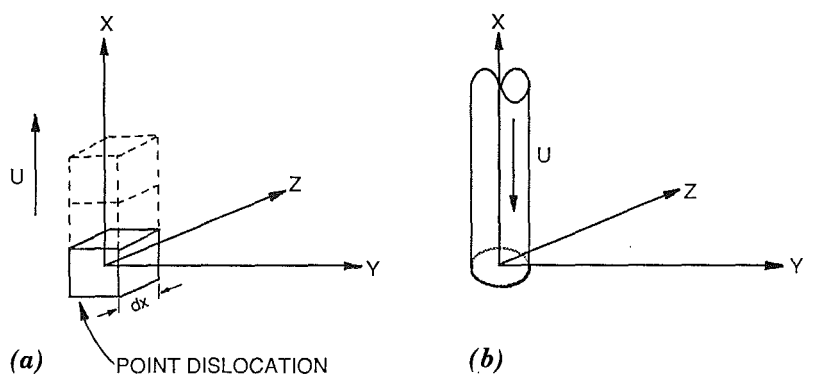

FIG. 1. Analogous Coordinate Systems: (*a*) Static Coordinate System within Traversing Medium; (*b*) Moving Coordinate System within Static Medium; Penetrometer

$$\bar{R}^2 = [x - U(t - \tau)]^2 + y^2 + z^2 \quad \ldots\ldots (2b)$$

where C_V = consolidation coefficient; k = permeability; and μ = dynamic viscosity to give the pore-water-pressure change above ambient ($p - p^s$) at time t and location x, y, x due to the point dislocation $vd\tau$ introduced at time τ.

In the preceding analysis the origin of the coordinate system remains coincident with the dilation introduced at current time level t. The correspondence between a fixed-coordinate system past which the medium moves at constant velocity U and a coordinate system moving at velocity $-U$ in a static medium is direct. For penetration of a rod of cross-sectional area a initiated at time $t = 0$ and progressing at rate U, the dilation rate is given as $v = Ua$. Substituting directly into Eq. 1 and integrating in time yields

$$p - p^s = \int_0^t \frac{C_V U a}{4\pi \bar{R}^3} \frac{\mu}{k} \left(\frac{\xi^{-3}}{2\sqrt{\pi}} e^{-\bar{\xi}^2/4} \right) d\tau \quad \ldots\ldots (3)$$

which on substitution of $\eta = R/2[C_V(t - \tau)]^{1/2}$; $a = \pi r^2$ for a rod of radius r; and with some rearrangement yields

$$p - p^s = \frac{\mu}{k} \frac{Ur^2}{2\pi^{1/2} R} e^{Ux/2C_V} \int_{R/2(C_V t)^{1/2}}^{\infty} e^{[-\eta^2 - (UR/4C_V\eta)^2]} d\eta \quad \ldots\ldots (4)$$

where $R^2 = x^2 + y^2 + z^2$. The integral must be evaluated numerically except for the steady conditions as $t \to \infty$ when the pressure distribution reduces to

$$p - p^s = \frac{\mu}{k} \frac{Ur^2}{4R} e^{-U(R-x)/2C_V} \quad \ldots\ldots (5)$$

Dimensionless Parameters

In considering induced pore pressures along the shaft only (i.e., $x \geq 0$; $y = z = 0$), then $R = x$; $0 < x < \infty$; and Eq. 5 conveniently yields a dimensionless pressure magnitude that asymptotes to unity as pore pressures reach a steady state in the vicinity of the penetrometer tip. Dimensionless pore pressure is recorded as

$$p_D = \frac{4(p - p^s)}{Ur} \frac{k}{\mu} \quad \ldots\ldots (6)$$

with

$$0.0 \leq P_D R_D \leq 1.0 \quad \ldots\ldots (7)$$

and

$$(x_D, y_D, z_D) = \frac{1}{r} (x, y, z) \quad \ldots\ldots (8)$$

and the product $P_D x_D$ may be considered equivalent to a normalized pore pressure used routinely in the analysis of piezocone data. To facilitate comparison with later results, the other dimensionless parameters of time t_D

$$t_D = \frac{4C_V t}{r^2} = \frac{R_D^2}{\xi^2} \quad \ldots\ldots (9)$$

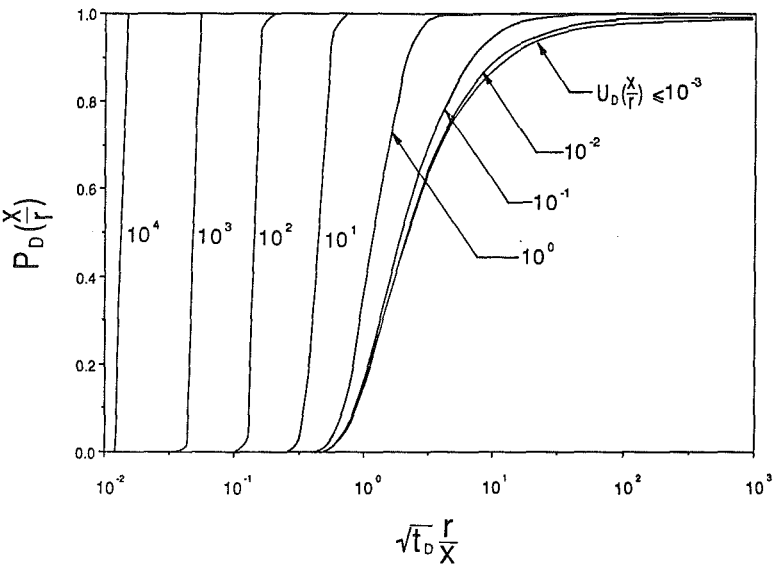

FIG. 2. Shaft Pore Pressures ($x \geq 0$; $y = z = 0$) Following Penetration Beginning at $t_D = 0$

with $R_D = R/r$; and penetration rate U_D

$$U_D = \frac{Ur}{2C_V} \quad \text{(10)}$$

are defined and standardized for the analysis.

From these definitions, the transient pore-pressure field identified in Eq. 4 may be recorded as

$$P_D R_D = \frac{2}{\sqrt{\pi}} \int_{R_D/t_D^{1/2}}^{\infty} e^{[U_D x_D - \eta^2 - (U_D R_D/2\eta)^2]} d\eta \quad \text{(11)}$$

and the steady pore-pressure distribution of Eq. 3 may be defined as

$$P_D R_D = e^{-U_D(R_D - x_D)} \quad \text{(12)}$$

using the simplified dimensionless terms.

Pore-Pressure Generation

The pore pressures along the shaft developed with penetration are illustrated in Fig. 2 for the only remaining dependent variables of Eq. 11. These are $U_D x_D$ and $\sqrt{t_D}/x_D$. Important points evident within the results are the following.

First, smaller dimensionless penetration rates U_D require a large dimensionless time to reach the steady condition at any designated location x_D along the shaft. This behavior is the essence of partially drained penetration.

Second, a threshold behavior is evident for dimensionless penetration rates $U_D x_D < 10^{-3}$, in which a single type curve represents the progress of pore-pressure generation. For penetration within a medium in which $U_D x_D$ is originally less than 10^{-3}, further decrease of the real penetration rate U does not affect the progress of pore-pressure generation in actual time. In this situation, only the absolute magnitude of the generated pore pressure $p - p^s$ is affected. Reducing the penetration rate by an order of magnitude identically reduces the generated pore pressures. For a full range of dimensionless penetration rates, a steady condition, with the establishment of peak pore-pressure magnitudes, is reached for $\sqrt{t_D}/x_D > 10^{-3}$. For fine-grained soils subjected to slow penetration, therefore, the time required to reach steady conditions may be excessive.

Third, large dimensionless penetration rates U_D give a rapid, sharp pressure response in dimensionless time. Phenomenologically, this response corresponds to the rapid movement of the pressure surrounding the dislocation tip. The exponential terms retained on the right-hand side of Eq. 4 replicate the characteristic form of the Heaviside function with a maximum value of unity at $t_D = 2\ x_D/U_D$. This location in dimensionless time represents the inflexion point of the pressure-time relationship that, for $U_D x_D \geq 10^3$, is ostensibly coincident with the near-vertical graph. Time to steady penetration may readily be evaluated from this parameter for large U_D.

Spatial Pressure Distribution

Although the time taken to reach the steady pore-pressure condition at any location along the shaft is dependent on the dimensionless penetration rate U_D, the resulting dimensionless shaft pore-pressure P_D is independent of U_D. This is evident from Eqs. 5 and 12, which reduce to $P_D x_D = 1.0$ for $R = x$ and $x \geq 0$. However, the spatial distribution of pore pressures surrounding the tip is strongly conditioned by penetration rate. This is most conveniently illustrated by the contoured distribution of pore pressures shown in Figs. 3 and 4.

Pore-pressure generation results are illustrated to an external radius of $0.10r$ in Fig. 3 and $10r$ in Fig. 4, for a range of dimensionless penetration rates spanning 10^6 to 10^{-4}. Results are reported for $t_D = 10^6$. The largest coordinate magnitude used in Fig. 4 is $x_D = 10$, resulting in a minimum magnitude $\sqrt{t_D}/x_D = 10^2$, effectively corresponding to the steady state for the included range of coordinate values. This detail may be readily confirmed from Fig. 2. Dimensionless axisymmetric coordinates are denoted $x_D = x/r$ and $y_D = y/r$ in Figs. 3 and 4.

Apparent at low penetration rates in the local geometric framework of Fig. 3 is the near-spherical distribution of the induced (and concurrently dissipating) pore-pressure field. The distribution is readily approximated by $P_D R_D = 1.0$ and remains virtually indistinguishable from this distribution for $U_D < 10^{-2}$. With increased penetration rate the distribution becomes successively more oblate, especially in the region ahead of the tip. This is first apparent for $U_D = 10^0$, and becomes more pronounced at higher penetration rates in which the lateral extent of the pressure distributions are uniquely described by dimensionless penetration rates when confined within the dimensionless coordinate system (x_D, y_D) illustrated in Fig. 3. The rate-dependent distribution of induced pressures further regulates the observed dissi-

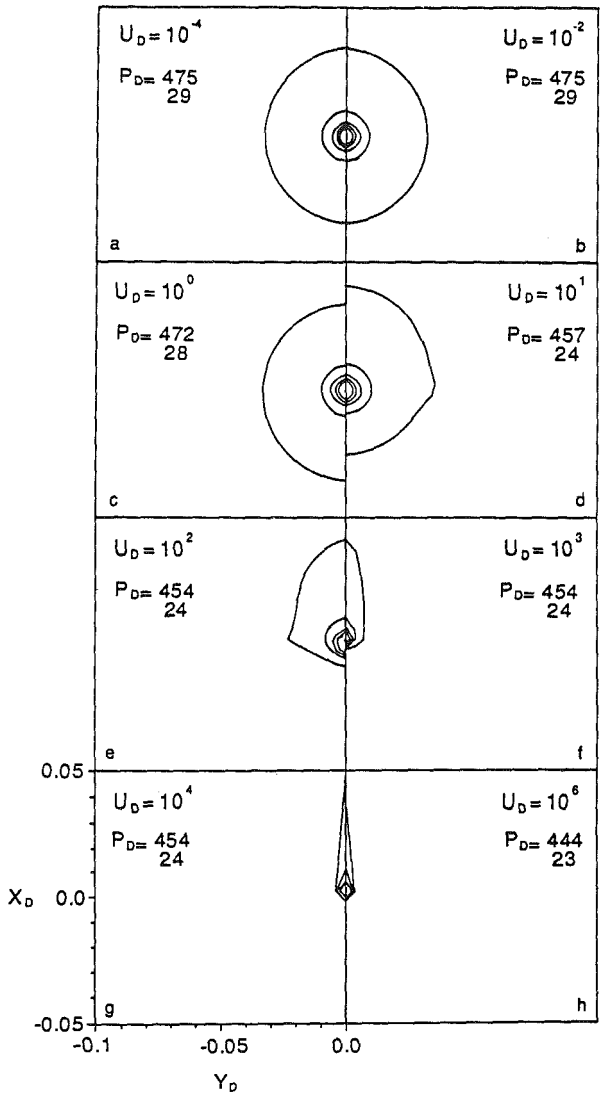

FIG. 3. Steady Pressure Distributions Proximal to Advancing Dislocation for Penetration Rates $10^{-4} \leq U_D \leq 10^{6}$

pation mechanisms and rates that proceed immediately following penetration arrest.

Contoured pressure distributions in the region enveloping the domain of Fig. 3 are illustrated in Fig. 4. The maximum lateral extent reaches y_D = 10. The change in morphology of the induced pore-pressure distribution from a spherical to an elongate form is apparent with increased penetration rate. The transition, however, occurs at lower penetration rates in the larger geo-

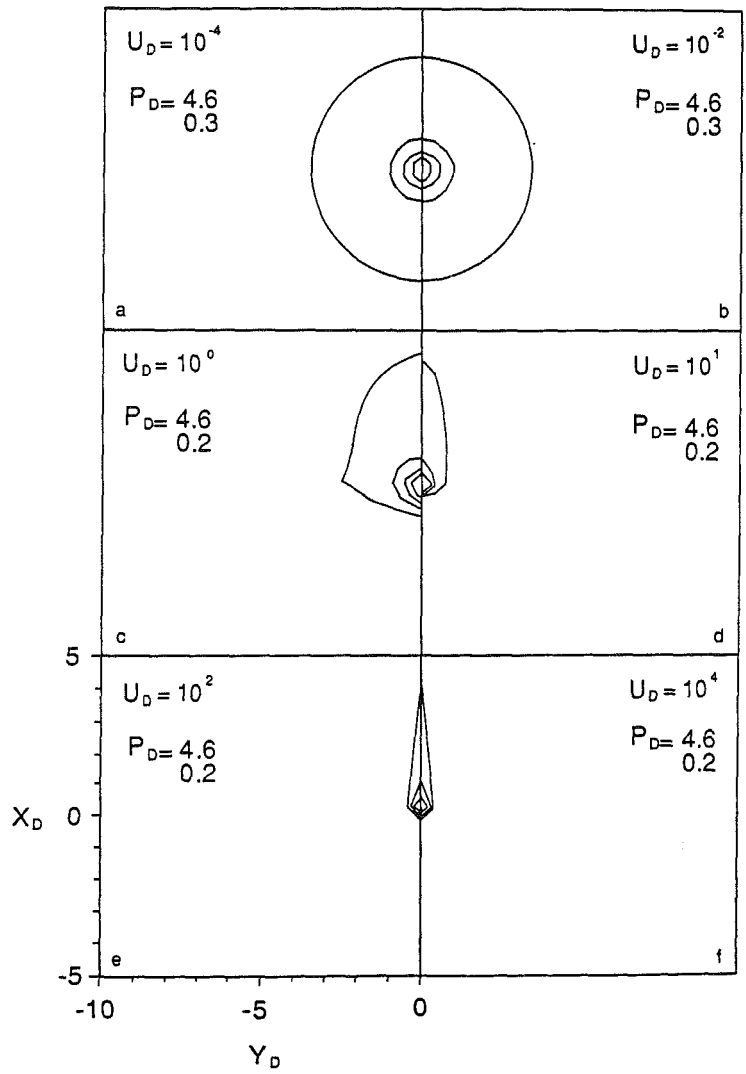

FIG. 4. Steady Pressure Distributions Distal from Advancing Dislocation for Penetration Rates $10^{-4} \leq U_D \leq 10^6$

metric setting. It may be corroborated from Fig. 2 that the entire extended domain has practically reached the steady condition at $t_D = 10^6$. There exists, therefore, a direct similitude between the steady-pressure conditions in the small and extended domains of Figs. 3 and 4, respectively. Increasing the spatial dimension by two orders of magnitude gives a two-orders-of-magnitude shift in the penetration rate required to return a specific pressure distribution. Pressure magnitudes are similarly reduced by a factor of 100. This behavior is confirmed through Eq. 12 by noting the functional dependence

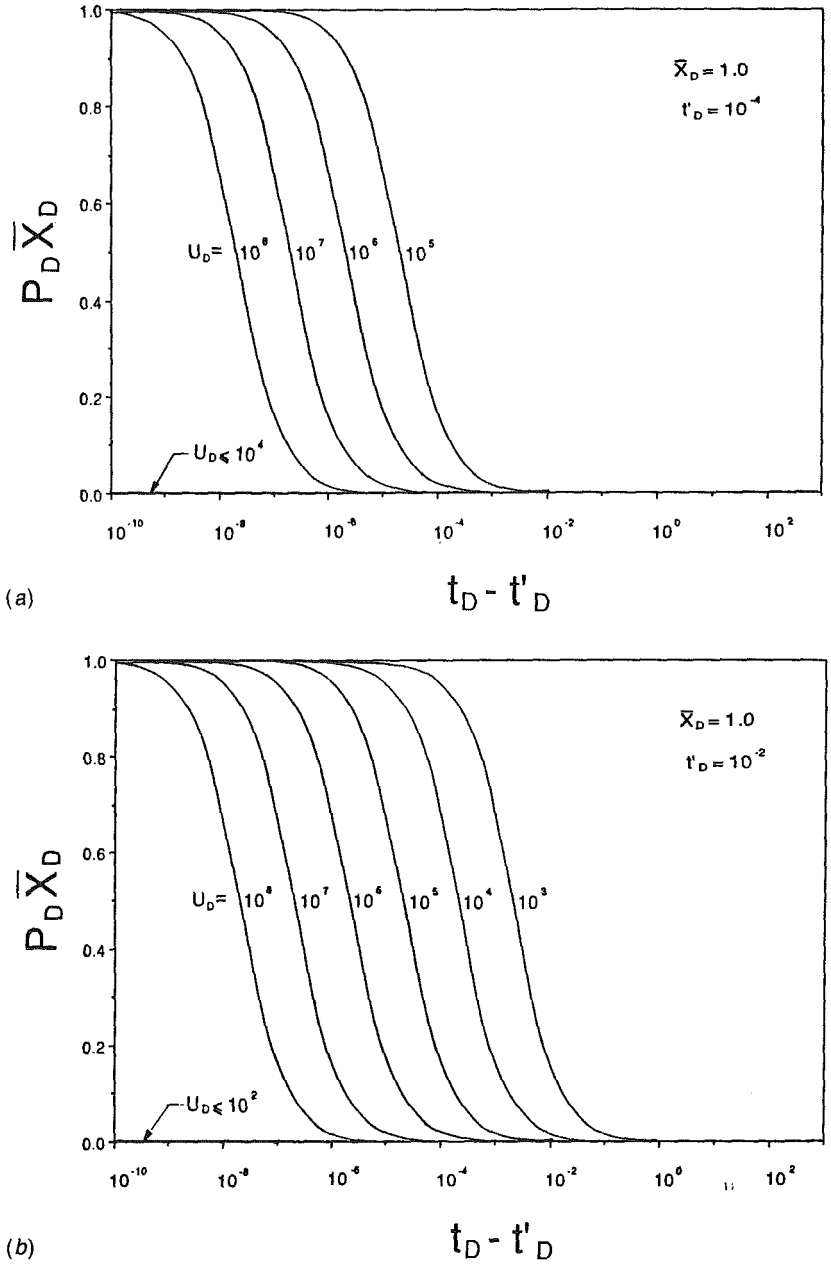

FIG. 5. Pore Pressure Responses of Shaft Following Dislocation Arrest at $10^{-4} \leq t_D \leq 10^4$ for Monitoring Location $x_D = 1.0$

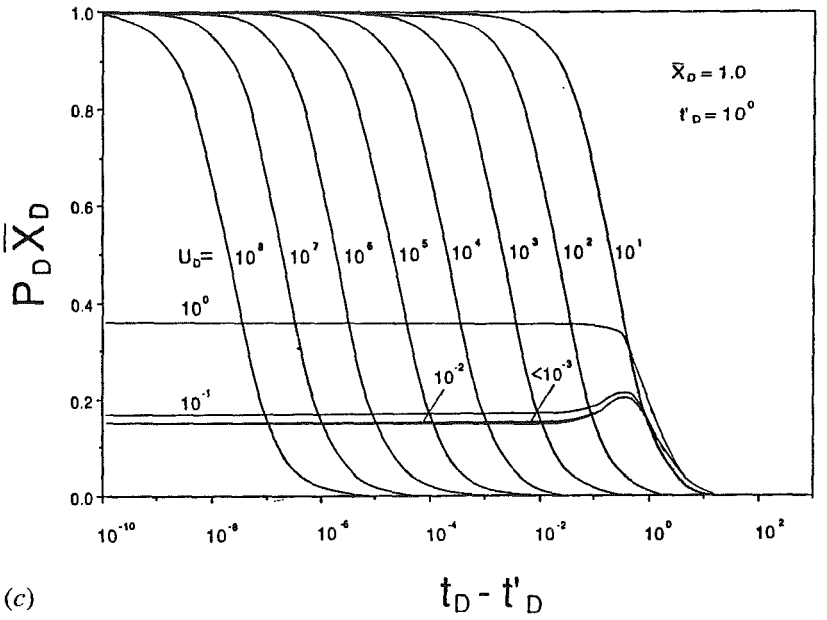

(*c*)

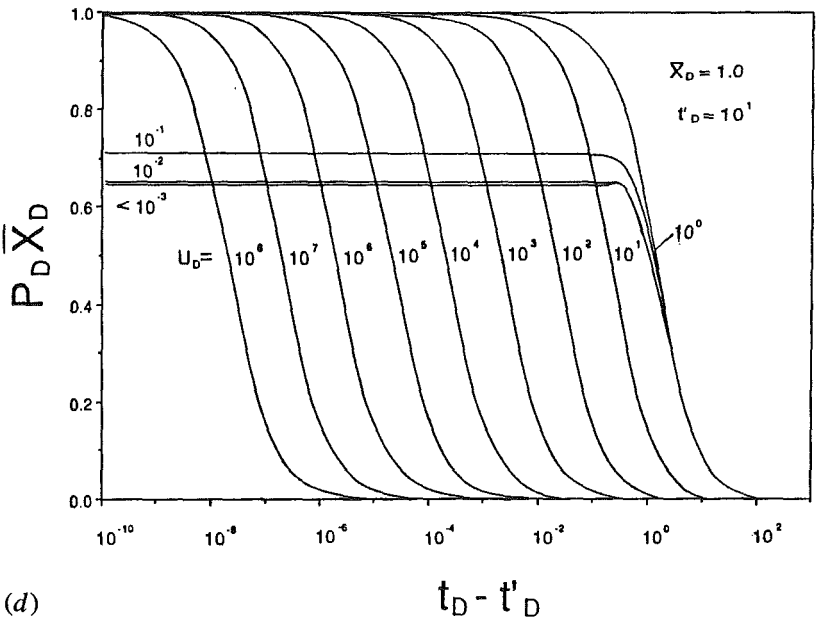

(*d*)

FIG. 5. (*Continued*)

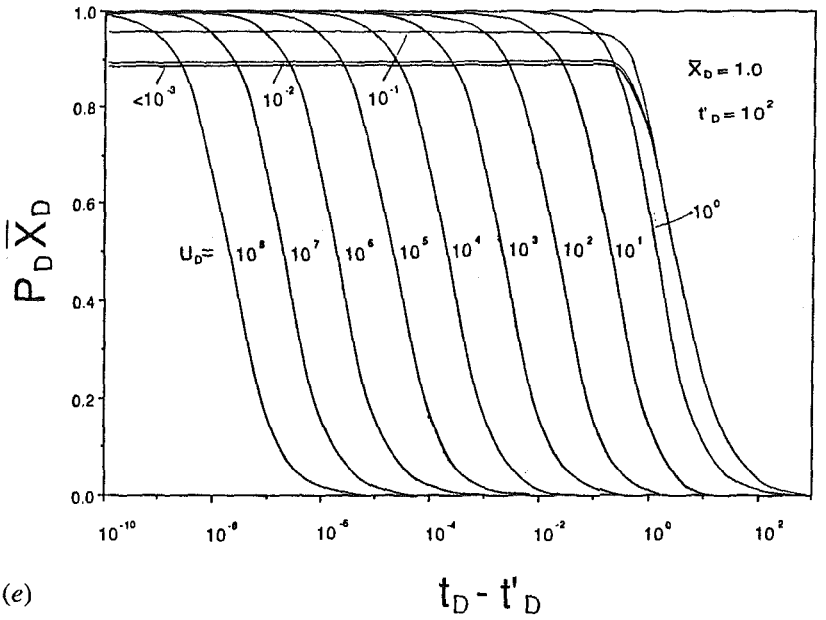

(*e*)

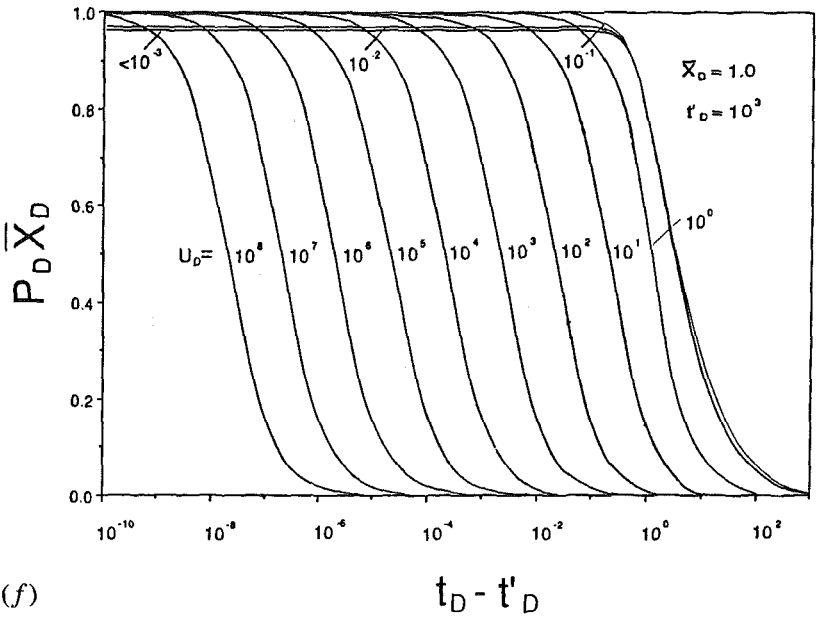

(*f*)

FIG. 5. (*Continued*)

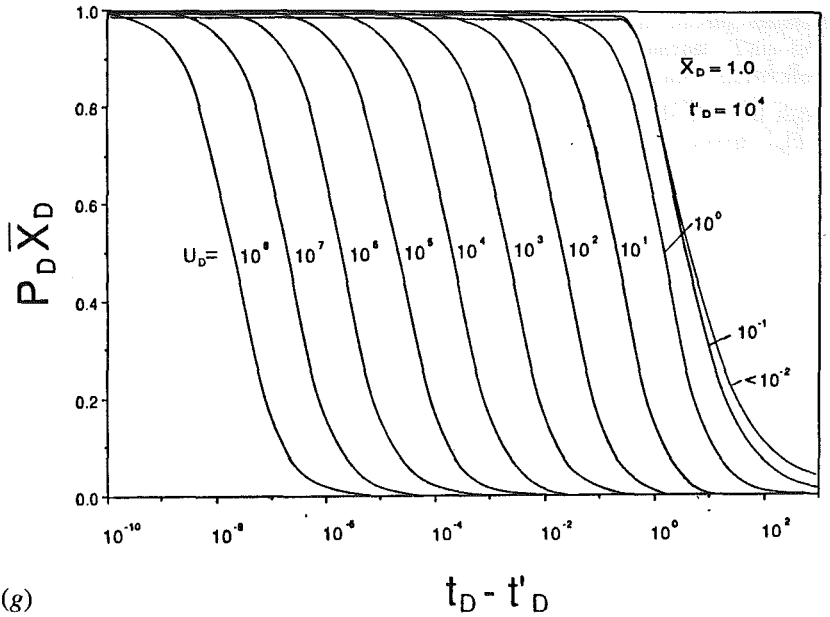

(*g*)

FIG. 5. (*Continued*)

of P_D and U_D upon the geometric parameters R_D and x_D. Thus, pressure distributions at any domain magnitude and corresponding penetration rate may be determined directly from Fig. 3 alone.

INTERRUPTED POINT DISLOCATION

The dissipation of pore pressures following arrest of a penetrometer may be evaluated by superposition. For penetration originating at time zero and arresting at time t', the pore-pressure dissipation at any subsequent time t ($t > t'$) is given by superposition of two concurrent and coincident moving-dislocation systems. The first system corresponds to a positive dislocation spanning the time interval $0 \rightarrow t$, and the second corresponds to a dislocation of equal strength and opposite sense spanning $t' \rightarrow t$. For this dual configuration of concurrently moving dislocations, the systems equation follows directly from Eq. 4 as

$$P_D R_D = \frac{2}{\sqrt{\pi}} e^{U_D x_D} \int_{R_D/t_D^{1/2}}^{R_D/(t_D - t'_D)^{1/2}} e^{[-\eta^2 - (U_D R_D/2\eta)^2]} \quad \ldots\ldots\ldots\ldots\ldots\ldots\ldots\ldots\ldots\ldots \quad (13)$$

where pressures are referenced relative to the continuously migrating coordinate system with $t'_D = 4C_v t'/r^2$. To obtain pressure distributions relative to the arrested penetration geometry, the coordinate system must be translated in the x-coordinate by substituting

$$x = \bar{x} - U(t - t') \quad \ldots\ldots\ldots\ldots\ldots\ldots\ldots\ldots\ldots\ldots\ldots\ldots\ldots\ldots\ldots\ldots \quad (14a)$$

$$y = \bar{y} \quad \text{(14b)}$$

$$z = \bar{z} \quad \text{(14c)}$$

with the bar denoting coordinates relative to the arrested geometry. In dimensionless form, the x-coordinate is defined

$$x_D = \bar{x}_D + \frac{1}{2} U_D(t_D - t'_D) \quad \text{(15)}$$

and retaining

$$R_D^2 = x_D^2 + y_D^2 + z_D^2 \quad \text{(16)}$$

enables Eq. 13 to be rewritten

$$P_D \bar{R}_D = \frac{\bar{R}_D}{R_D} \frac{2}{\sqrt{\pi}} e^{U_D x_D} \int_{R_D/t_D^{1/2}}^{R/(t_D - t'_D)^{1/2}} e^{[-\eta^2 - (U_D R_D/2\eta)^2]} d\eta \quad \text{(17)}$$

where $\bar{R}_D = R_D$ at time $t_D = t'_D$ representing the desired location relative to the penetrometer at the time of arrest. Eq. 17 is entirely general and allows the pressure distribution to be determined in dimensionless coordinates $(\bar{x}_D, \bar{y}_D, \bar{z}_D)$. Setting $t_D = t'_D$ further allows pre-arrest pressure distributions to be evaluated and, in this instance, Eqs. 17 and 4 are clearly equivalent.

Pressure Dissipation Response

The dissipation of pore pressures measured along the shaft of the instrument ($\bar{x}_D > 0$) is controlled by the dimensionless groupings

$$P_D \bar{x}_D = f\left(\frac{t'_D}{\bar{x}_D^2}; \frac{t_D - t'_D}{\bar{x}_D^2}; U_D \bar{x}_D\right) \quad \text{(18)}$$

Thus, in presenting the results for measured pore-pressure dissipation of the dimensionless shaft pressure magnitudes, $P_D \bar{x}_D$, may be plotted against dimensionless time following penetrometer arrest, $(t_D - t'_D)/\bar{x}_D^2$, for a variety of dimensionless penetration rates, $U_D x_D$. These groupings neglect the influence of the time prior to penetration arrest $(t'_D/\bar{x}_D^2)$ and require that a separate plot be presented for increasing magnitudes of $t'_D/\bar{x}_D^2$, as illustrated in the sequence of Figs. 5(a–g) for $10^{-4} \leq t'_D/\bar{x}_D^2 \leq 10^4$. These figures record dimensionless pore pressures $P_D \bar{x}_D$ at a shaft location $\bar{x}_D = 1.0$, and therefore $U_D \bar{x}_D = U_D$ and $(t_D - t'_D)/\bar{x}_D^2 = (t_D - t'_D)$. Individual figures represent a range of penetration-arrest times spanning $10^{-4} \leq t'_D \leq 10^4$. The following important observations may be made from these data.

Dissipation records obtained from the dislocation analysis are not independent of the penetration rate that generated the primary pore-pressure field. This corollary may be surmised from the contour results of Fig. 3 and is the essence of partially drained penetration behavior. Importantly, this contradicts the contention that a single (unique) response curve, fixed in dimensionless time, may adequately represent dissipation of pore pressures on the shaft.

Premature arrest (at very low $t'_D/\bar{x}_D^2$ values) may result in the absence of some dissipation records. This is evident in Fig. 5(a), in which records rep-

resenting $U_D\bar{x}_D \leq 10^4$ are absent as a result of insufficient time having elapsed to generate significant pore pressures at the location of interest. This behavior may be corroborated from the pressure-generation records illustrated in Fig. 2. Increasing the time to penetrometer arrest by two orders of magnitude, to $t'_D/\bar{x}_D^2 = 10^{-2}$ as illustrated in Fig. 5(*b*), adds a further two dissipation records, spanning two orders of magnitude in the dimensionless penetration rate $U_D\bar{x}_D$.

With a further increase in the duration of steady penetration, records that are partway between the null pressure and the steady conditions are apparent, as illustrated for $U_D\bar{x}_D \leq 10^0$ in Fig. 5(*c*).

Similar to the generation of pore pressures, a threshold dissipation behavior is apparent for $U_D\bar{x}_D \leq 10^{-3}$ as a result of identical initial pressure distributions preceding the dissipation process. This behavior is apparent in Figs. 5(*c–g*).

Swelling behavior is observed in limited circumstances for $U_D\bar{x}_D \leq 10^{-1}$, in which penetration is arrested at $t'_D/\bar{x}_D^2 = 10^0$, prior to the attainment of the steady state, as evident in Fig. 5(*c*). This effect disappears as penetration arrest is further delayed, and is not apparent in the record for arrest at $t'_D/\bar{x}_D^2 = 10^1$.

With increased penetration duration, the steady-state pressure distribution is more readily attained. The pressure transient records of Figs. 5(*f* and *g*), corresponding to the arrest times $t'_D/\bar{x}_D^2 = 10^3$ and 10^4, respectively, are virtually indistinguishable. These pressure records represent a unique set for arrest times greater than $t'_D/\bar{x}_D^2 = 10^4$. It is confirmed that pressure-dissipation records remain sensitive to penetration rates irrespective of whether a steady pressure distribution is attained prior to arrest.

For dimensionless penetration rates $U_D\bar{x}_D$ smaller than 10^{-2}, a single pressure-dissipation response is evident in Fig. 5(*g*). This response is unique for all smaller penetration rates and is fixed within dimensionless time. For rapid penetration rates, the pressure transient responses are similar and offset in time by constant magnitude. The temporal shift corresponds to a single-order-of-magnitude acceleration in response to an order-of-magnitude increase in penetration rate.

Spatial Pressure Dissipation

Functional dependence of the spatial distribution of pore-pressure dissipation is uniquely controlled by the groupings

$$P_D\bar{R}_D = f\left(\frac{t'_D}{\bar{x}_D^2}; \frac{t_D - t'_D}{\bar{x}_D^2}; U_D\bar{x}_D; \frac{\bar{y}_D}{\bar{x}_D}\right) \quad (19)$$

Thus the distribution of P_D may be recorded with location for a variety of penetration rates U_D. The dissipation response is controlled by the dimensionless time parameter $(t_D - t'_D)/\bar{x}_D^2$, with the responses for identical penetration rate magnitudes $U_D\bar{x}_D$ being equivalent, provided $t'_D/\bar{x}_D^2$ is large enough to ensure the establishment of an initial steady pore-pressure distribution.

Records of spatial pressure distributions following penetration arrest are illustrated in Figs. 6 and 7. The contoured results are illustrated for the dissipation response following penetration at dimensionless rates $U_D = 10^{-2}$, 10^0, 10^2, and 10^6, ostensibly at steady state at the instant of penetration arrest $t'_D = 10^6$. Prearrest penetration rates of $10^{-2} \leq U_D \leq 10^6$ span the full spec-

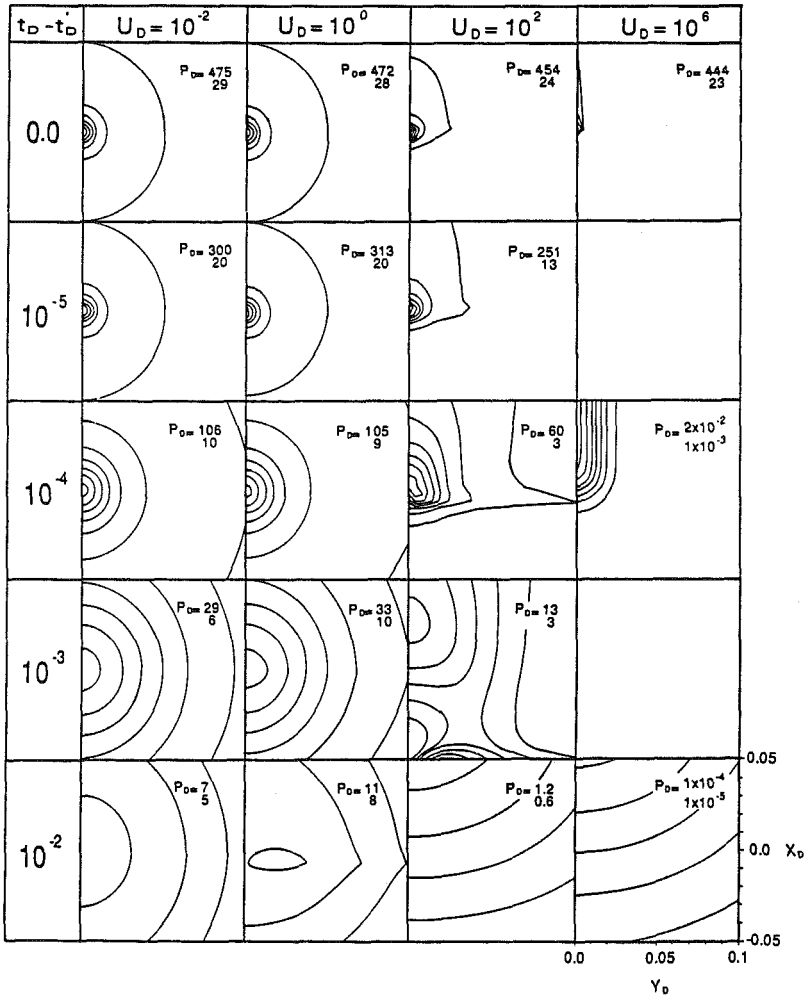

FIG. 6. Spatial Pressure-Dissipation Records Proximal to Arrested Dislocation for Penetration Rates $10^{-2} \leq U_D \leq 10^{6}$ Arrested at $t'_D = 10^{6}$

trum of pressure generation and the subsequent dissipation mechanism encompassing the transition from spherical to radial morphologies with increased penetration rate. The dissipation processes are viewed at small (Fig. 6) and large (Fig. 7) scale relative to the dimensionless spatial coordinate system $(\bar{x}_D, \bar{y}_D)$.

Considering first the reduced domain, Fig. 6 illustrates the manner in which dissipation morphology is affected by the prearrest penetration rate U_D. The pressure distributions generated at low penetration rates of $U_D = 10^{-2}$ and $U_D = 10^{0}$ retain their spherical form throughout the dissipation process. The cusp feature exhibited in the dissipation form for $U_D = 10^{0}$ at large elapsed time marks the transition from spherical symmetry at $U_D \leq 10^{0}$ to the "ham-

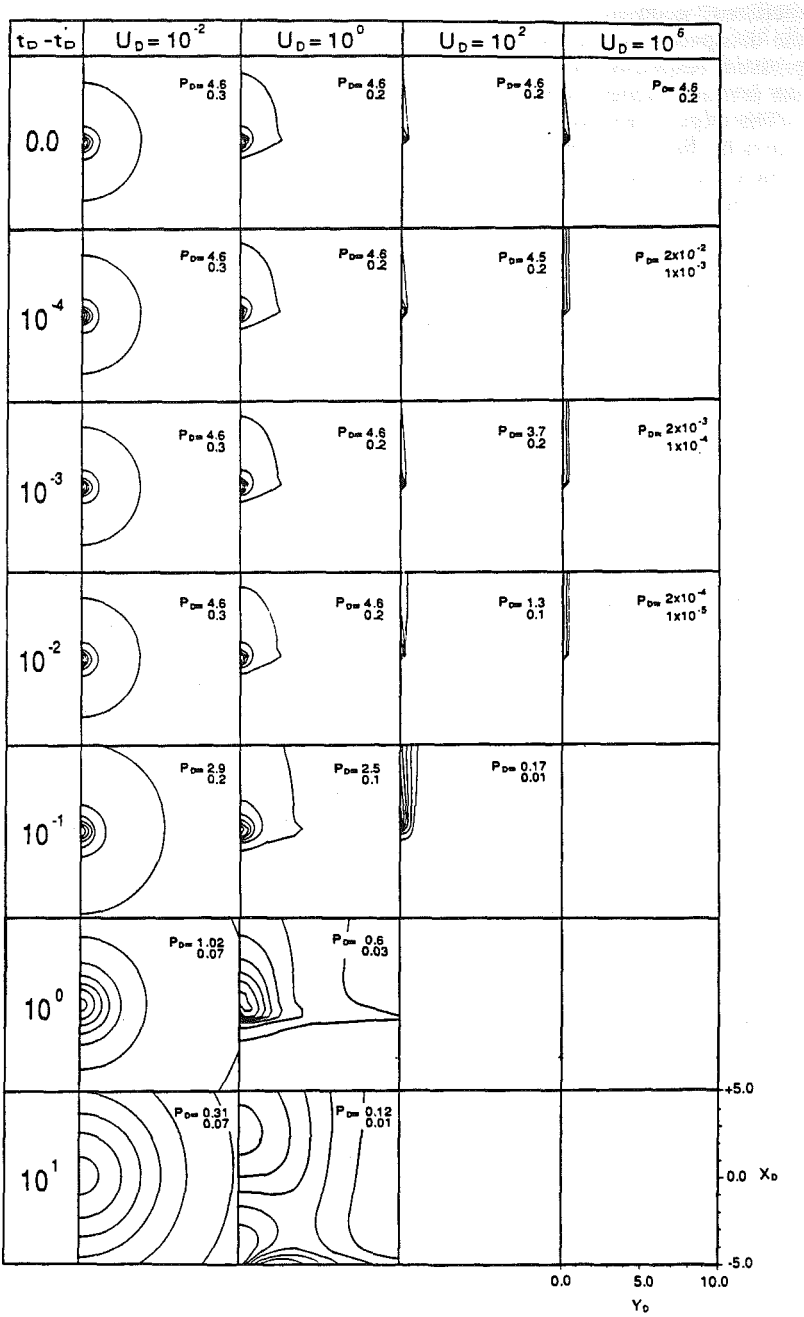

FIG. 7. Spatial Pressure-Dissipation Records Distal from Arrested Dislocation for Penetration Rates $10^{-2} \leq U \leq 10^{6}$ Arrested at $t'_D = 10^{6}$

merhead" geometry for $U_D = 10^2$. As penetration rate is further increased the dissipation geometry becomes radial for $U_D = 10^6$. As predicted by the pressure response curves of Fig. 5, the rate of dissipation is accelerated as the prearrest penetration rate increases.

The larger contoured geometry, illustrated in Fig. 7, marks the same transition in dissipation processes from spherical to purely radial form, as exhibited in the reduced domain of Fig. 6. The full geometric extent of the contoured domain in Fig. 6 represents a small area surrounding the origin; and it is fully contained within Fig. 7. As a direct consequence, the contoured pressure magnitudes cover a significantly reduced range in the more extensive geometry, although the singular behavior at the origin, prearrest, remains apparent. Indeed, changing the scale of observation in the area surrounding the arrested tip indicates that both spherical and radial pressure-dissipation mechanisms may progress simultaneously. This is apparent on comparing Figs. 6 and 7 for the single penetration rate of $U_D = 10^0$. Clearly, when viewed at large scale, the dissipation process is radial whereas local to the tip, the dissipation process retains a spherical form.

Conclusions

Solution is presented to the problem of a point-normal dislocation moving within a saturated, porous-elastic medium. The analogy with cone penetration is clear; however, departure from the true physical system is apparent in that the dislocation is reduced to a point, of infinitesimal dimension, and that linear elastic behavior is assumed in the surrounding medium.

The important points to be distilled from the preceding are the following:

The dislocation method allows prediction of the elapsed time required to reach a steady pressure response at any shaft-monitoring location. For $U_D x_D \geq 10^3$ the time to reach 50% of the steady pressure ($0.5 P_D x_D$) is given by $t_D = x_D(2/U_D)$. For $U_D x_D \geq 10^3$ the pressure response is so rapid that for all practical purposes the 50% response time also represents the time to reach the steady pressure. For small penetration rates with $U_D x_D \leq 10^{-2}$, the time to reach 50% of the steady pressure is given by $\sqrt{t_D}/x_D = 2.065$, and to reach 95% of steady pressure the time is given by $\sqrt{t_D}/x_D = 25.586$.

Under steady conditions, the shaft pressure distribution is given by $P_D \bar{x}_D = 1.0$. Since all the parameters comprising $P_D \bar{x}_D$ are known or may be readily evaluated excepting the magnitude k/μ, it is feasible that permeability magnitudes may be recovered directly from the measured pressure response. This is only applicable if steady conditions have been reached.

Penetration-generated pore-pressure distributions are strongly influenced by penetration rate U_D. The generated pressure bulb is of spherical form for low penetration rates and develops an elongate distribution as penetration rate increases.

For dissipation analysis the functional relationship

$$P_D \bar{x}_D = f\left(\frac{t'_D}{\bar{x}_D^2}; \frac{t_D - t'_D}{\bar{x}_D^2}; U_D \bar{x}_D; \frac{\bar{y}_D}{\bar{x}_D}\right) \quad \text{..... (20)}$$

uniquely controls the process. For shaft pressures, $\bar{y}_D/\bar{x}_D = 0$ and an individual set of type curves must, in theory, be provided for all required values of arrest time $t'_D/\bar{x}_D^2$. At large magnitudes of arrest time, however, the steady

condition is reached prior to arrest and a single set of curves will suffice.

Particular caution should be taken in the use of pressure buildup and dissipation responses recorded along the penetrometer shaft. The problems of nonuniqueness engendered in the analysis are especially disturbing and worthy of further field documentation. Recognition of the behavioral limitations of the dislocation theory is crucial to successful application of the theory in the reduction of penetrometer data.

The preceding observations promote a fundamental understanding of the processes operating during piezocone penetration and arrest. Together they provide the potential for obtaining maximum information from piezocone pressure records, including direct determination of fluid permeability and compressibility coefficients.

Acknowledgments

The support of the National Science Foundation under Grant MSM-8708976 is most gratefully acknowledged.

Appendix I. References

Acar, Y. B., and Tumay, M. T. (1986). "Strain field around cones in steady penetration." *J. of Geotech. Engrg.*, ASCE, 112(2), 207–213.

Baligh, M. M., and Scott, R. F. (1976). "Analysis of wedge penetration in clay." *Géotechnique,* London, England, 26(1), 185–208.

Baligh, M. M. (1985). "Strain path method." *J. Geotech. Engrg.*, ASCE, 111(9), 1108–1136.

Battaglio, M., Jamidkowki, M., Lancellotta, R., and Maniscalco, M. (1981). "Piezometer probe test in cohesive deposits." *Proc., Symp. on Cone Penetration Testing and Experience,* ASCE, New York, N.Y., 264–302.

Biot, M. A., and Willis, D. G. (1957). "The elastic coefficients of the theory of consolidation." *J. Appl. Mech.*, 24, 594–601.

Carter, J. P., Booker, J. R., and Yeung, S. K. (1986). "Cavity expansion in cohesive-frictional soils." *Géotechnique,* London, England, 36(3), 349–358.

Cleary, M. P. (1977). "Fundamental solutions for a fluid-saturated porous solid." *Int. J. Solids Structures,* 13(9), 785–806.

Drescher, A., and Kang, M. (1987). "Kinematic approach to limit load for steady penetration in rigid-plastic soils." *Géotechnique,* London, England, 37(3), 233–246.

Gupta, R. C., and Davidson, J. L. (1986). "Piezoprobe determined coefficient of consolidation." *Soils and Found.*, 26(3), 12–22.

Janbu, N., and Senneset, K. (1974). "Effective stress interpretation of in situ static penetration tests." *Proc., European Symp. on Penetration Testing, I,* Stockholm.

Jones, G. A., and Van Zyl, D. J. A. (1981). "The piezometer probe—a useful investigation tool." *Proc., 10th Int. Conf. on Soil Mech. and Found. Engrg. (ICSMFE),* Stockholm, 2, 489–496.

Ladanyi, B. (1963). "Expansion of a cavity in a saturated clay medium." *J. Soil Mech. and Found. Div.*, ASCE, 89(4), 127–161.

Skempton, A. W. (1954). "The pore-pressure coefficients A and B." *Géotechnique,* London, England, 4, 143–147.

Torstensson, B. A. (1975). "Pore pressure sounding instrument." *Proc., ASCE Specialty Conf. on In Situ Measurement in Soil Properties,* ASCE, New York, N.Y., 2, 48–54.

Tumay, M. T., Acar, Y. B., Cekirge, M. H., and Ramesh, N. (1985). "Flow field around cone in steady penetration." *J. Geotech. Engrg.*, ASCE, 111(2), 193–204.

Appendix II. Notation

The following symbols are used in this paper:

a = penetrometer shaft cross-sectional area $a = \pi r^2$;
C_V = consolidation coefficient;
k = intrinsic permeability;
P_D = dimensionless pressure;
p = total fluid pressure;
p^s = initial static fluid pressure;
R = radius of interest $R^2 = x^2 + y^2 + z^2$;
r = penetrometer shaft radius;
t = time (current);
t_D = dimensionless time (current);
t' = time of penetration arrest;
t'_D = dimensionless time of penetration arrest;
U = penetration rate;
U_D = dimensionless penetration rate;
V = volume change due to dislocation;
v = dislocation magnitude introduced in time $d\tau$;
x, y, z = global Cartesian coordinates;
$\bar{x}, \bar{y}, \bar{z}$ = Cartesian coordinates relative to arrested geometry;
x_D, y_D, z_D = dimensionless Cartesian coordinates (x/r; y/r; z/r);
η = integration coefficient;
μ = fluid dynamic viscosity;
ξ = dimensionless inverse root time $\xi = R/\sqrt{C_V t}$; and
τ = time integrating parameter.